PHYSICAL REVIEW B **86**, 064205 (2012)

Electrical, magnetic, and thermal properties of the δ-$FeZn_{10}$ complex intermetallic phase

S. Jazbec,[1] P. Koželj,[1] S. Vrtnik,[1] Z. Jagličić,[2] P. Popčević,[3] J. Ivkov,[3] D. Stanić,[3,*] A. Smontara,[3] M. Feuerbacher,[4] and J. Dolinšek[1,5,†]

[1]*J. Stefan Institute & University of Ljubljana, Faculty of Mathematics and Physics, Jamova 39, SI-1000 Ljubljana, Slovenia*
[2]*Institute of Mathematics, Physics and Mechanics & University of Ljubljana, Faculty of Civil and Geodetic Engineering, Jadranska 19, SI-1000 Ljubljana, Slovenia*
[3]*Institute of Physics, Bijenička 46, POB 304, HR-10001 Zagreb, Croatia*
[4]*Institut für Festkörperforschung, Forschungszentrum Jülich, Jülich D-52425, Germany*
[5]*EN-FIST Centre of Excellence, Dunajska 156, SI-1000 Ljubljana, Slovenia*

(Received 9 July 2012; published 23 August 2012)

We report the electrical, magnetic, and thermal properties of the δ-$FeZn_{10}$ phase in the zinc-rich domain of the Fe-Zn system. The δ-$FeZn_{10}$ phase possesses high structural complexity typical of complex metallic alloys: a giant unit cell comprising 556 atoms, polyhedral atomic order with icosahedrally coordinated environments, fractionally occupied lattice sites, and statistically disordered atomic clusters that introduce intrinsic disorder into the structure. Structural disorder results in suppression of the electrical and heat transport phenomena, making δ-$FeZn_{10}$ a poor electrical and thermal conductor. Structural complexity results in a complex electronic structure that is reflected in the opposite signs of the thermoelectric power and the Hall coefficient. The δ-$FeZn_{10}$ phase is paramagnetic down to the lowest investigated temperature of 2 K with a significant interspin coupling of antiferromagnetic type. Specific heat indicates the formation of short-range-ordered spin clusters at low temperatures, very likely a precursor of a phase transition to a collective magnetic state that would take place below 2 K. The magnetoresistance of δ-$FeZn_{10}$ is sizeable, amounting to 1.5% at 2 K in a 9-T field. The electrical resistivity exhibits a maximum at about 220 K, and its temperature dependence could be explained by the theory of slow charge carriers, applicable to metallic systems with weak dispersion of the electronic bands, where the electron motion changes from ballistic to diffusive upon heating.

DOI: 10.1103/PhysRevB.86.064205 PACS number(s): 72.15.Eb, 75.47.Np, 65.40.Ba

I. INTRODUCTION

The term "complex metallic alloys" (CMAs) denotes a class of intermetallic phases with giant unit cells containing hundreds to many thousands of atoms.[1] Examples of CMAs are the cubic $NaCd_2$ with 1152 atoms per unit cell (u.c.),[2,3] the Bergman phase $Mg_{32}(Al,Zn)_{49}$ (162 atoms/u.c.),[4] the orthorhombic ξ'-$Al_{74}Pd_{22}Mn_4$ (318 atoms/u.c.), and the related Ψ phase (about 1500 atoms/u.c.),[5–7] the cubic β-Al_3Mg_2 (1168 atoms/u.c.),[8–10] the hexagonal λ-Al_4Mn (586 atoms/u.c.),[11] the $Al_{39}Fe_2Pd_{21}$ (248 atoms/u.c.),[12] the heavy-fermion compound $YbCu_{4.5}$ (7448 atoms/u.c.),[13] and the $cF(23, 256\text{-}x)$-$Al_{55.4}Cu_{5.4}Ta_{39.1}$ phase of great complexity, comprising more than 23 000 atoms in the unit cell.[14] These giant unit cells contrast with elementary metals and simple intermetallics whose unit cells usually comprise single atoms to a few tens of atoms only. The giant unit cells with lattice parameters of several nanometers provide translational periodicity of the CMA crystalline lattice on the scale of many interatomic distances, whereas on the atomic scale, the atoms are arranged in clusters with polyhedral order, where icosahedrally coordinated environments play a prominent role. The structures of CMAs thus show duality; on the scale of several nanometers, CMAs are periodic crystals, whereas on the atomic scale some of them resemble quasicrystals.[15] The high structural complexity of CMAs together with the two competing physical length scales—one defined by the unit-cell parameters and the other by the cluster substructure—may have a significant impact on the physical properties of these materials, such as the electronic structure and lattice dynamics. Recently, the structure of a CMA was reported in the zinc-rich domain of the Fe-Zn system,[16] the δ-$FeZn_{10}$ phase, which comprises 556 atoms in the giant hexagonal unit cell arranged in a very dense packing of icosahedra and a few other polyhedra. The physical properties of the δ-$FeZn_{10}$ phase remain unknown, and it is the purpose of this work to report on the electrical, magnetic, and thermal properties of this interesting CMA.

II. STRUCTURAL CONSIDERATIONS AND SAMPLE DESCRIPTION

The zinc-rich domain of the Fe-Zn system between 67 and 95 at% Zn has been intensely studied in the past,[17–20] owing to its technological importance in the field of anticorrosion techniques. It comprises several different phases, among which the δ phase exists in the homogeneity range between 86.5 and 92 at% Zn (at 300 °C). A structural model has been elaborated for the composition $FeZn_{10}$,[16] showing that δ-$FeZn_{10}$ crystallizes in the hexagonal space group $P6_3/mmc$ (No. 194) with the lattice constants $a = 1.2787$ nm and $c = 5.7222$ nm and 556 atoms in the giant unit cell (52 Fe and 504 Zn). The unit cell contains 47 Zn and 5 Fe crystallographic sites, seven of which are fractionally occupied [the sites Zn(46), Fe(47), Fe(49), Zn(50), Zn(51), and Fe(52) by 1/3 and the site Fe(48) by 2/3, according to the nomenclature of Ref. 16. The structure can be viewed as very dense packing of four types of polyhedra (Fig. 1): (1) a statistically disordered distorted icosahedron centered on the Zn(40) atom and spinning around a threefold axis inside a large Euler polyhedron containing 40 atoms and having 76 faces and 114 edges; (2) a Frank–Kasper 16-vertex

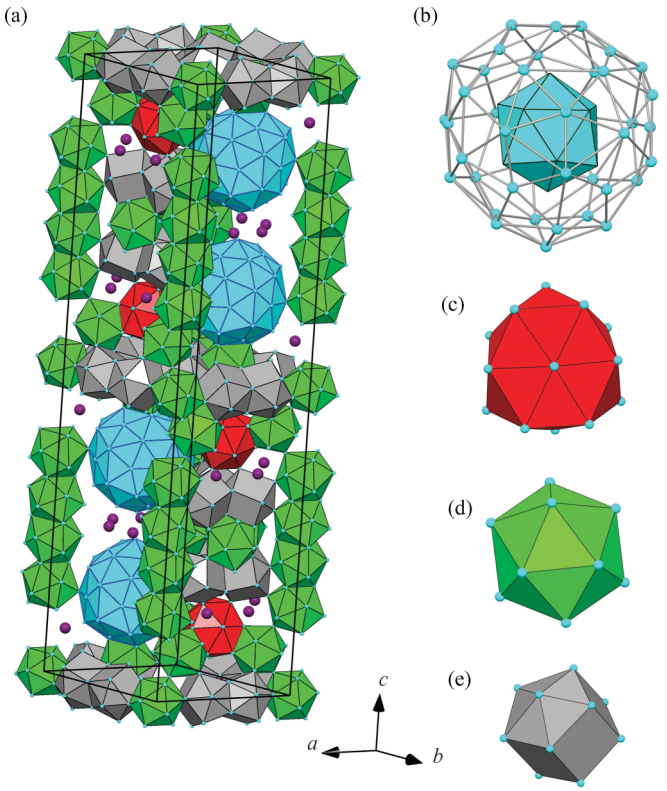

FIG. 1. (Color online) (a) δ-$FeZn_{10}$ hexagonal unit cell according to the structural model of Ref. 16. The structure can be viewed as very dense packing of four types of polyhedra, (b) a statistically disordered, distorted icosahedron inside a large Euler polyhedron (blue/medium gray), (c) a Frank–Kasper 16-vertex polyhedron, also referred to as the icosioctahedron (red/dark gray), (d) a more or less regular icosahedron (green/light gray), and (e) a bicapped pentagonal prism (gray online). The remaining "glue" atoms are shown violet (dark gray).

polyhedron, also referred to as the icosioctahedron; (3) a more or less regular icosahedron (bicapped pentagonal antiprism); and (4) a bicapped pentagonal prism. The seven fractionally occupied sites are all located on the statistically disordered distorted icosahedron and introduce randomness and intrinsic disorder into the structure. This icosahedron also contains all Fe sites.

Our δ-$FeZn_{10}$ material was synthesized by the self-flux method under conditions similar to those described in Ref. 16. A sample of dimensions $1 \times 1 \times 3\ mm^3$ was extracted from the ingot. Structural characterization by x-ray diffraction (XRD), scanning electron microscopy (SEM), and transmission electron microscopy (TEM) techniques has shown that the sample was single phase and contained several grains, so it should be considered as a polygrain material.

III. EXPERIMENTAL RESULTS

Magnetic measurements were conducted by a Quantum Design Magnetic Property Measurement System (MPMS) XL-5 superconducting quantum interference device (SQUID) magnetometer equipped with a 5-T magnet, operating in the temperature range 2–400 K. The measurements of the electrical resistivity, the magnetoresistance, the thermal conductivity, and the specific heat were conducted by a Quantum Design Physical Property Measurement System (PPMS 9T), equipped with a 9-T magnet and operating in the temperature range 2–400 K. The electrical resistivity and the magnetoresistance were measured by a standard four-terminal technique. The thermal conductivity was measured by monitoring the temperature drop across the sample after a heat pulse was applied to its end by means of square waves. The specific heat was measured by a thermal-relaxation calorimeter. The thermoelectric power was measured between 300 and 2 K in a homemade cryostat by applying a differential method with two identical thermocouples (chromel-gold with 0.07% iron), attached to the sample with silver paint. The Hall coefficient measurements were performed by the five-point method using standard ac technique in magnetic fields up to 1 T and in the temperature interval between 370 and 90 K.

A. Magnetization and magnetic susceptibility

The magnetic susceptibility $\chi = M/H$ was determined in the temperature range 2–300 K in several magnetic fields up to $H = 10$ kOe. χ was found to be field independent, and in Fig. 2(a) it is presented in the $H = 1$-kOe field. The analysis with the Curie–Weiss law

$$\chi = \chi_0 + \frac{C}{T - \theta} \tag{1}$$

in the high-temperature range $T > 100$ K (solid curve) yielded the temperature-independent contribution $\chi_0 = 2.5 \times$

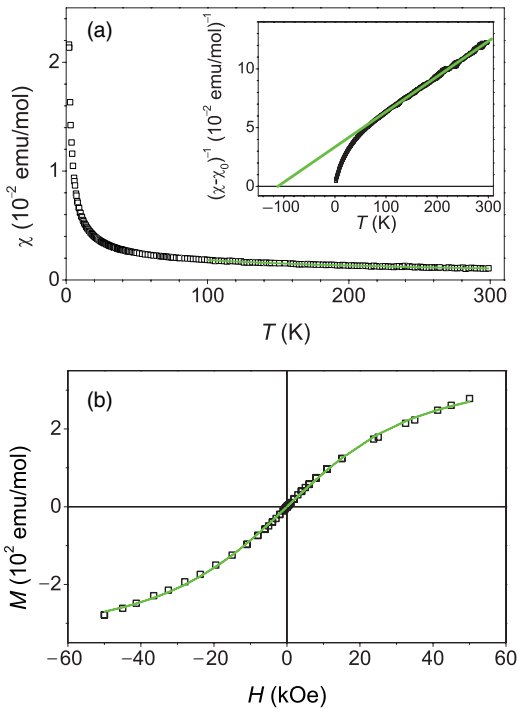

FIG. 2. (Color online) (a) Temperature-dependent magnetic susceptibility $\chi = M/H$ of δ-$FeZn_{10}$ in a magnetic field $H = 1$ kOe. Solid curve is the Curie–Weiss fit for temperatures $T > 100$ K. The inset shows the susceptibility in a $(\chi - \chi_0)^{-1}$ versus T plot, where the Curie–Weiss fit is presented by the straight line. (b) The magnetization versus the magnetic field, $M(H)$, at $T = 5$ K. Solid curve is the fit with Eq. (2).

10^{-4} emu/mol, the Curie–Weiss constant $C = 0.33$ emu K/mol, and the Curie–Weiss temperature $\theta = -112$ K, where χ_0 and C are given per mole Fe. The Larmor diamagnetic susceptibility of closed atomic shells was calculated from literature tables to amount $\chi_{\rm dia} = -1.1 \times 10^{-4}$ emu/mol of sample so that the positive χ_0, which is of the same order of magnitude as $|\chi_{\rm dia}|$, can be interpreted to originate predominantly from the Pauli spin susceptibility of the conduction electrons (the Landau diamagnetic contribution due to the conduction electron orbital circulation can be neglected because of the relatively high electrical resistivity of the δ-$FeZn_{10}$ material, as we shall demonstrate in the following). The Curie–Weiss constant C enables extraction of the mean effective Bohr magneton number per Fe atom, which amounts to $\bar{p}_{\rm eff} = 1.6$. This value is significantly reduced with respect to the Bohr magneton numbers of free ions Fe^{2+} ($p = 5.4$) and Fe^{3+} ($p = 5.9$), showing that the Fe magnetic moments in the δ-$FeZn_{10}$ phase are partially screened by the conduction-electron cloud in an electrically conducting environment. The rather large negative value of the Curie–Weiss temperature θ suggests relatively strong antiparallel (antiferromagnetic, AFM-type) coupling between the Fe moments. In the inset of Fig. 2(a), the susceptibility data are presented in a $(\chi - \chi_0)^{-1}$ versus T plot, where the Curie–Weiss fit is presented by the straight line and the intercept of this line with the abscissa yields negative θ. That graph also suggests that the validity of the Curie–Weiss law is restricted to temperatures $T > 70$ K.

The magnetization versus the magnetic field relation, $M(H)$, was determined at $T = 5$ K and is shown in Fig. 2(b). The data were analyzed by the function

$$M = M_0 B_J(\mu H/k_B T) + kH. \quad (2)$$

Here M_0 is the saturation magnetization, B_J is the Brillouin function, describing the response of localized paramagnetic moments of angular momentum J to the external magnetic field, and $\mu = Jg\mu_B$ is their magnetic moment, where μ_B is the Bohr magneton and g is the Landé factor (taken as $g = 2$). The parameter k represents terms in the susceptibility $\chi = M/H$ that are linear in the magnetic field (the Larmor, the Pauli, and the Landau contributions). It should be in principle the same as the temperature-independent contribution χ_0 in the Curie–Weiss susceptibility so that in the fit procedure we have used the $k = \chi_0$ value determined previously from the Curie–Weiss fit. The theoretical fit [solid curve in Fig. 2(b)] was obtained with the parameter values $M_0 = 250$ emu/mol and $J = 2.2$. This J value is intermediate to the values expected for the Fe^{2+} ($J = 2$) and Fe^{3+} ($J = 2.5$) ionizations states (under the condition of quenched orbital angular momentum, $L = 0$).

Magnetic measurements show that the δ-$FeZn_{10}$ phase remains paramagnetic down to the lowest investigated temperature of 2 K. Its magnetism originates from both the localized Fe moments and the spins of the conduction electrons. The Fe moments are reduced with respect to the free-ion values due to partial screening by the conduction-electron cloud, and their coupling is antiparallel (AFM type).

B. Electrical resistivity

The electrical resistivity of δ-$FeZn_{10}$ was measured between 300 and 2 K, and the $\rho(T)$ data are displayed in Fig. 3.

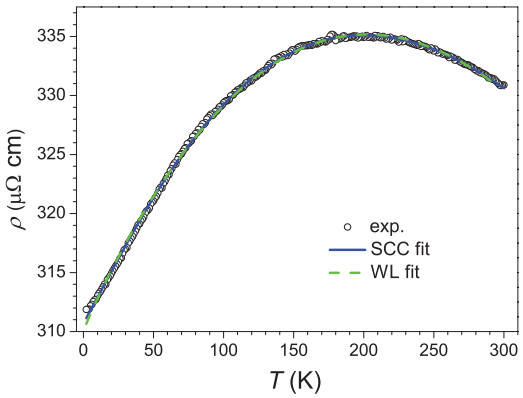

FIG. 3. (Color online) Temperature-dependent electrical resistivity of δ-$FeZn_{10}$ between 300 and 2 K. Solid curve (blue) is the theoretical fit with the model of SCC, whereas the dashed curve (green) is the fit with the model of WL. The fit parameters are given in the text.

The resistivity exhibits broad maximum at about 220 K. The room-temperature (RT) value amounts to $\rho_{300\,\rm K} = 331\ \mu\Omega$ cm, the value in the maximum is $\rho_{220\,\rm K} = 335\ \mu\Omega$ cm, whereas the resistivity in the $T \to 0$ limit remains large, amounting to $\rho_{2\,\rm K} = 312\ \mu\Omega$ cm. The overall variation of the resistivity between 2 K and the maximum is rather small, amounting to $(\rho_{220\,\rm K} - \rho_{2\,\rm K})/\rho_{2\,\rm K} = 7\%$.

The temperature dependence of the electrical resistivity that exhibits a maximum will be discussed in Sec. IV. Here it is worth mentioning that the large residual $T \to 0$ resistivity of $\rho_{T\to 0} \approx 310\ \mu\Omega$ cm reflects quenched intrinsic disorder in the lattice due to fractionally occupied sites in the unit cell and the presence of the statistically disordered icosahedron in the structure, which locally break the translational periodicity and consequently increase the resistivity. This effect is a peculiarity of CMAs and quasicrystals, where even the most perfect samples may contain an intrinsic disorder that is a part of the structure, needed for its entropic stabilization.

C. Magnetoresistance

To determine the magnetoresistance of δ-$FeZn_{10}$, the electrical resistivity was measured in a magnetic field up to 9 T. In Fig. 4(a), the resistivity $\rho(T)$ is shown in the temperature range from 100 to 2 K in the magnetic field varying in steps of $\Delta B = 1$ T. The temperature-dependent magnetoresistance $\Delta\rho/\rho = [\rho(B) - \rho(0)]/\rho(0)$ in $B = 9$ T is shown in the inset of Fig. 4(b), where it is observed that $\Delta\rho/\rho$ remains nonzero almost up to RT and reaches 1.5% at 2 K. The magnetic field dependence of $\Delta\rho/\rho$ at the temperatures 2, 5, 10, 20, and 50 K is shown in Fig. 4(b). The magnetoresistance will be discussed in Sec. IV.

D. Thermoelectric power

The thermoelectric power data (the Seebeck coefficient S) of δ-$FeZn_{10}$, measured between 300 and 2 K, are displayed in Fig. 5. The thermopower is small, amounting to $S_{300\,\rm K} = -1\ \mu$V/K at RT, and negative, suggesting that the electrons are the majority charge carriers. $S(T)$ exhibits a local minimum at about 70 K and a local maximum at 160 K. The rather

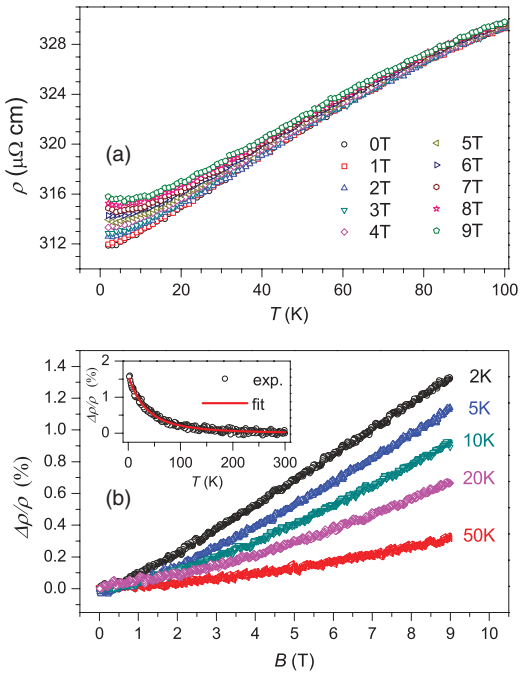

FIG. 4. (Color online) (a) The resistivity $\rho(T)$ of δ-FeZn$_{10}$ in the temperature range between 100 and 2 K in the magnetic field varying in steps of $\Delta B = 1$ T. (b) Magnetic field dependence of the magnetoresistance $\Delta\rho/\rho = [\rho(B) - \rho(0)]/\rho(0)$ at temperatures 2, 5, 10, 20, and 50 K. The inset shows the temperature-dependent magnetoresistance $\Delta\rho/\rho$ in $B = 9$ T between RT and 2 K. Solid curve is the fit with Eq. (7).

complicated temperature dependence of $S(T)$ may originate from both the complexity of the Fermi surface and the electron-phonon coupling (phonon drag).

E. Hall coefficient

The temperature-dependent Hall coefficient $R_H = E_y/j_x B_z$ of δ-FeZn$_{10}$ was determined between 370 and 90 K and is shown in Fig. 6. The R_H values are typically metallic in the range 10^{-10} m^3 C^{-1} with the experimental precision of $\pm 0.1 \times 10^{-10}$ m^3 C^{-1} and positive in the entire investigated

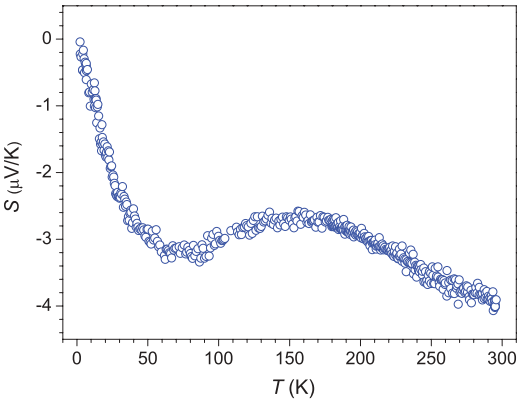

FIG. 5. (Color online) Temperature-dependent thermoelectric power (the Seebeck coefficient S) of δ-FeZn$_{10}$ between 300 and 2 K.

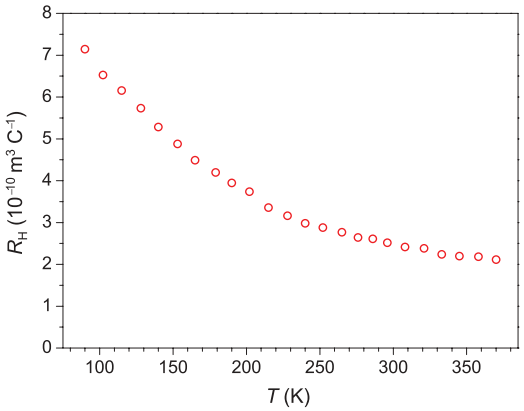

FIG. 6. (Color online) Temperature-dependent Hall coefficient R_H of δ-FeZn$_{10}$ between 370 and 90 K.

temperature range, suggesting that holes are the majority charge carriers. R_H increases upon cooling by a factor 3.5 from 380 to 90 K, but the values remain in the metallic range so that this relatively small increase may be attributed to the temperature-dependent changes of the Fermi surface. The opposite signs of the thermopower and the Hall coefficient will be discussed in Sec. IV.

F. Specific heat

The specific heat $C(T)$ of δ-FeZn$_{10}$ will be a sum of the electronic, lattice, and magnetic contributions. The electronic specific heat depends linearly on temperature, $C_{el}(T) = \gamma T$, with the electronic specific-heat coefficient $\gamma = (\pi^2/3)k_B^2 g(\varepsilon_F)$, where $g(\varepsilon_F)$ is the electronic density of states (DOS) at the Fermi energy ε_F. At low temperatures below $\sim$10 K, the lattice specific heat can usually be well approximated by the Debye model and is expressed as a function of temperature in the form $C_{\text{latt}}(T) = \alpha T^3$. The lattice specific heat coefficient α is related to the Debye temperature via the relation $\theta_D = (12\pi^4 R/5\alpha)^{1/3}$, where R is the gas constant. The magnetic specific heat C_m depends on the type of magnetic state. The total specific heat at low temperatures can be written as

$$C(T) = \gamma T + \alpha T^3 + C_m(T). \quad (3)$$

If the magnetic contribution $C_m(T)$ would be vanishing small, the coefficients γ and α can be determined from the zero intercept and slope of the straight line in a C/T versus T^2plot of the data, yielding $g(\varepsilon_F)$ and θ_D. For a significant $C_m(T)$, such analysis is inadequate.

The specific-heat measurements were performed in the temperature range between 2 and 300 K in magnetic fields $B = 0$ and 9 T. The low-temperature specific heat below 5 K is displayed in Fig. 7 in a C/T versus T^2plot, whereas the specific heat in the entire investigated temperature range is displayed in the inset. The difference between the zero-field and the 9-T specific heats is observed only at the lowest investigated temperatures below about 3.5 K, where the specific heat in zero field is enhanced with respect to the one in 9 T. Although there are several possible explanations of this enhancement effect, the most plausible one seems to be the magnetic contribution to the specific heat due to the

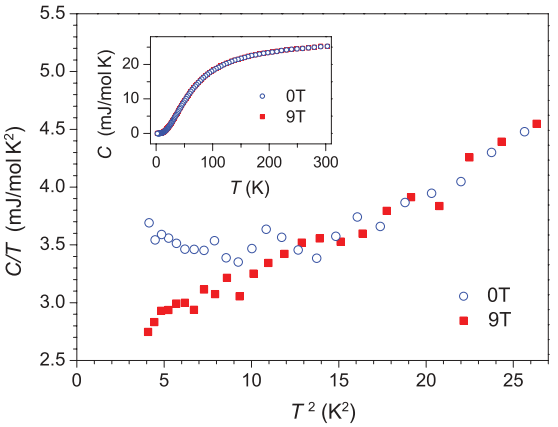

FIG. 7. (Color online) Low-temperature specific heat of δ-$FeZn_{10}$ in magnetic fields 0 and 9 T in a C/T versus T^2 plot. The inset shows specific heat in the entire investigated temperature range from RT to 2 K.

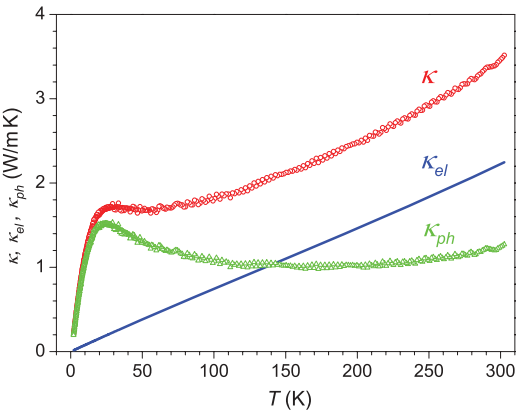

FIG. 8. (Color online) Thermal conductivity κ of δ-$FeZn_{10}$ between 300 and 2 K. The decomposition of the total thermal conductivity κ into the electronic κ_{el} and the phononic κ_{ph} parts by using the WF law is shown as well.

appearance of magnetic short-range order on approaching a phase transition to a collective magnetic state, which would take place below our lowest investigated temperature of 2 K. The large negative value of the Curie–Weiss temperature ($\theta = -112$ K) suggests a relatively strong AFM-type exchange coupling between the Fe moments so that an AFM magnetic ordering (or spin-glass type, due to intrinsic disorder in the δ-$FeZn_{10}$ phase) can be expected to take place at temperatures low enough that the exchange interactions will prevail over the thermal disordering of the spins. The hypothesis of short-range spin ordering at low temperatures is supported by the response of the specific heat to the magnetic field. The Zeeman interaction of the spins with the external field opposes the tendency of the formation of short-range-ordered AFM-type spin clusters, which diminishes the magnetic contribution to the specific heat in the field, as also observed experimentally.

Since the δ-$FeZn_{10}$ compound consists mainly of the Zn element (its chemical formula can also be written as $Fe_{0.09}Zn_{0.91}$), it is instructive to compare the magnitude of C/T at the lowest investigated temperature of 2 K to the magnitude of the electronic specific-heat coefficient γ of the Zn metal. From Fig. 7 we read the zero-field value $(C/T)^{0\,\mathrm{T}}_{2\,\mathrm{K}} = 3.7\ \mathrm{mJ/mol \cdot K^2}$, whereas the 9-T value is $(C/T)^{9\,\mathrm{T}}_{2\,\mathrm{K}} = 2.8\ \mathrm{mJ/mol \cdot K^2}$. The electronic specific-heat coefficient of the Zn metal is[21] $\gamma_{\mathrm{Zn}} = 0.638\ \mathrm{mJ/mol \cdot K^2}$. The inequality $(C/T)_{2\,\mathrm{K}} > \gamma_{\mathrm{Zn}}$ cannot be explained by the difference in the DOSs of the two materials (since the electrical resistivity of the Zn metal is two orders of magnitude smaller than the resistivity of δ-$FeZn_{10}$, the DOS of Zn is larger and the opposite inequality should hold in that case) but should be attributed to the magnetic specific-heat contribution of iron in the δ-$FeZn_{10}$. Due to the significant, yet not well-defined $C_m(T)$ contribution, the coefficients γ and α cannot be determined reliably from the data analysis with Eq. (3).

G. Thermal conductivity

Thermal conductivity κ of δ-$FeZn_{10}$ between 300 and 2 K is shown in Fig. 8. κ shows a typical phonon umklapp maximum at about 25 K and a continuous increase above 100 K, reaching a low value $\kappa_{300\,\mathrm{K}} = 3.5$ W/mK at RT. Since the electrical resistivity of this material is also high for an intermetallic compound, δ-$FeZn_{10}$ is a poor conductor for both the electricity and the heat. The low electrical and thermal conductivities of the δ-$FeZn_{10}$ phase have a simple explanation by considering the intrinsic disorder-induced suppression of the electron and phonon propagation in the crystalline lattice.

The phononic thermal conductivity $\kappa_{ph} = \kappa - \kappa_{el}$ can be estimated by subtracting the electronic contribution κ_{el} from the total conductivity κ using the Wiedemann–Franz (WF) law, $\kappa_{el} = \pi^2 k_B^2 T/3\rho(T)e^2$, and the measured electrical resistivity data $\rho(T)$ from Fig. 3. Here it is important to recall the validity of the WF law,[22] which is valid under the condition of dominant elastic scattering of the electrons. This is usually realized at high temperatures $T > \theta_D$, whereas at low temperatures, the WF law is valid for solids where only the residual electrical resistivity (due to elastic scattering by quenched defects) is observed. Inspecting the electrical resistivity of the δ-$FeZn_{10}$ from Fig. 3, we observe that this material exhibits very large residual resistivity and a relatively small temperature-dependent resistivity change (by 7% at most) between 2 K and RT. This suggests that the elastic scattering by quenched disorder provides an important contribution to the total resistivity of the intrinsically disordered δ-$FeZn_{10}$ phase. The WF law could thus be considered as an approximation to $\kappa_{el}(T)$, although we should keep in mind that its validity is compromised by the observation of the inelastic scattering effects in the temperature-dependent electrical resistivity (to be discussed in Sec. IV).

The decomposition of the total thermal conductivity κ into the electronic κ_{el} and the phononic κ_{ph} parts by using the WF law is shown in Fig. 8. κ_{ph} exhibits a plateau above the umklapp maximum, a consequence of frequent phonon scattering by the quenched structural disorder that diminishes the lattice thermal conductivity. At 300 K we obtain the values $\kappa_{el} = 2.2$ W/mK and $\kappa_{ph} = 1.3$ W/mK. This yields the ratio $(\kappa_{el}/\kappa)_{300\,\mathrm{K}} = 0.63$ so that the electrons (and holes) are the dominant heat carriers at 300 K.

IV. DISCUSSION

A. Electrical resistivity

We discuss here two theoretical approaches that can reproduce the maximum in the temperature-dependent electrical resistivity and are applicable to systems that contain intrinsic disorder and compromised translational periodicity such as CMAs and quasicrystals. The first is the theory of quantum transport of slow charge carriers (the SCC model),[23] and the second is the theory of weak localization (the WL model) of conduction electrons in a disordered medium.[24] In the following we apply both models to the electrical resistivity of δ-$FeZn_{10}$ from Fig. 3 and show that they reproduce the experimental $\rho(T)$ data to practically equal precision. However, while the application of the SCC model can be justified at any temperature, the WL model is restricted to low temperatures with no clear indication at which temperature it breaks down.

1. Slow charge carriers

The SCC model[23] is based on the weak dispersion of the electronic band energies $E_n(\vec{k})$, where n is the band index and $\vec{k}$ the wave vector, in which case the electron velocity $\vec{v} = (1/\hbar)\partial E_n(\vec{k})/\partial\vec{k}$ is small. The model predicts a transition from ballistic (Boltzmann) to diffusive (non-Boltzmann) electrical conductivity as a function of the relaxation time τ between the electron scattering events that enters the electron mean-free path $l = v\tau$. The electrical conductivity (the inverse resistivity, $\sigma = \rho^{-1}$) is given by the Einstein relation $\sigma = e^2 g(\varepsilon_F) D$, where $g(\varepsilon_F)$ is the DOS at ε_F and D is the electronic diffusion constant that can be written by simple kinetic arguments as $D = v^2\tau/3 = l^2/3\tau$, with v^2 being the mean-square electronic speed. For long τ, usually realized at low temperatures, the mean-free path l between the scattering events is larger than the extension of the conduction-electron wave packet L_{wp} so that the motion of electrons is ballistic, and one obtains in the free-electron limit the Drude conductivity $\sigma = ne^2\tau/m$. Since τ shortens upon raising the temperature, this yields a positive-temperature-coefficient (PTC) resistivity in the low-temperature ballistic regime. At higher temperatures, τ becomes short enough to drive the system into the $l \approx L_{wp}$ limit of diffusive type of motion. The diffusion constant then becomes inversely proportional to the relaxation time, $D = L^2/\tau$, where L is a constant proportional to the elementary diffusion step. This yields the conductivity of the type $\sigma \propto 1/\tau$ that results in a nonmetallic negative-temperature-coefficient (NTC) resistivity in the high-temperature regime. At the transition from the ballistic to the diffusive type of motion, the resistivity exhibits a maximum and a crossover from the low-T PTC to the high-T NTC resistivity. The temperature of the resistivity maximum depends sensitively on the electronic velocity v (hence on the electronic structure and band dispersion) and the temperature-dependent relaxation time $\tau(T)$. Various possible temperature-dependent electrical resistivities within the SCC model (PTC, NTC, and mixed PTC-NTC with a maximum), expressed by the formula of the form

$$\rho^{-1} = A\tau + B/\tau, \tag{4}$$

were elaborated theoretically in detail in a previous publication (see Fig. 7 of Ref. 25). The SCC model has been successfully applied to the temperature-dependent resistivities of the Al_4(Cr,Fe) decagonal approximant,[25,26] the giant-unit-cell heavy-fermion compound $YbCu_{4.25}$,[27] the μ-Al_4Mn complex intermetallic,[28] and the resistivity in the quasiperiodic plane of the d-Al-Co-Ni decagonal quasicrystal[29] that all exhibit a maximum.

The relaxation rate τ^{-1} will generally be a sum of a temperature-independent rate τ_e^{-1} due to elastic scattering by quenched defects and a temperature-dependent rate τ_i^{-1} that contains any inelastic scattering processes, e.g., the scattering by phonons. In the simplest case, τ_i can be phenomenologically written as a power law of the temperature, $\tau_i = \beta/T^\alpha$, at least within a limited temperature interval. Equation (4) can then be cast into the form[25]

$$\rho^{-1} = \frac{A}{1 + CT^\alpha} + B\,(1 + CT^\alpha), \tag{5}$$

where $A = e^2 g(\varepsilon_F) v^2 \tau_e$, $B = e^2 g(\varepsilon_F) L^2/\tau_e$ and $C = \tau_e/\beta$. Equation (5) contains four fit parameters A, B, C, and α (where the last two always appear in a product CT^α). Equation (5) was used to fit the resistivity of δ-$FeZn_{10}$, and the resulting theoretical curve is shown in Fig. 3 as a solid curve. Excellent agreement with the experiment was found in the entire investigated temperature range, reproducing well the maximum of the resistivity. The fit parameters are $A = 2.2 \times 10^{-3}\,(\mu\Omega\,\mathrm{cm})^{-1}$, $B = 1.0 \times 10^{-3}\,(\mu\Omega\,\mathrm{cm})^{-1}$, $C = 1.6 \times 10^{-3}$, and $\alpha = 1.1$, where the units of C are chosen such that the temperature in the expression CT^α appears dimensionless.

2. Weak localization

In "dirty" metals with strong electronic scattering, the interference between scattered waves is important. Since the elastic scattering time τ_e is independent of temperature, whereas the inelastic scattering time $\tau_i(T)$ increases with decreasing temperature, there exists a region, usually limited to low temperatures, where the inequality $\tau_e \ll \tau_i$ holds. In such a case, several elastic scattering events take place within one inelastic scattering event, and different types of interference effects occur: weak localization and enhanced electron-electron interactions.[24] WL is a one-electron effect in which the elastically scattered electron interferes with itself during the time of preserved phase coherence, usually taken to be the inelastic scattering time. This leads to an increased tendency towards backscattering, from which the terminology of weak localization has been coined. Weak localization introduces small temperature-dependent correction $\Delta\sigma_{WL}(T)$ to the Boltzmann conductivity due to spin-orbit and inelastic scattering processes of the electrons. The conductivity is written in the form

$$\begin{aligned}\sigma &= \sigma_0 + \Delta\sigma_{WL}(T) \\ &= \sigma_0 + \frac{e^2}{2\pi^2\hbar\sqrt{D\tau_{so}}}(3\sqrt{t+1} - \sqrt{t} - 3),\end{aligned} \tag{6}$$

where σ_0 is the residual conductivity in the $T \to 0$ limit, D is the diffusion constant, τ_{so} the spin-orbit scattering time, and $t = \tau_{so}/4\tau_i(T)$, where $\tau_i(T)$ is the inelastic scattering time that

can be taken in the form $\tau_i \propto 1/T^{\alpha}$ [the same form as used in Eq. (5) of the SCC model]. The WL model also yields a maximum in the temperature-dependent electrical resistivity, which is a consequence of the interplay between the spin-orbit and the inelastic scattering processes of the conduction electrons. The fit of the δ-$FeZn_{10}$ resistivity data with Eq. (6) is shown in Fig. 3 by a dashed curve, using the parameter values $\sigma_0 = 3.2 \times 10^{-3}$ $(\mu\Omega\,\mathrm{cm})^{-1}$, $e^2/(2\pi^2\hbar\sqrt{D\tau_{so}}) = 1.4 \times 10^{-3}$ $(\mu\Omega\,\mathrm{cm})^{-1}$, and by rewriting $t = (T/T_0)^{\alpha}$, $T_0 = 608$ K, and $\alpha = 1.9$. The WL fit is excellent, and moreover, it gives an indistinguishable curve to the SSC fit.

The WL and the SCC theories thus fit the experimental resistivity data of the δ-$FeZn_{10}$ to equal precision. This raises the question whether the two theories are in essence the same, despite different starting hypotheses, or the perfect matching of the two theoretical curves in Fig. 3 is accidental, caused by a relatively large number of free parameters in the fit procedure (four in both cases). Here it should be emphasized that the applicable temperature ranges for the WL and the SCC models are different. The limiting factor for when the WL effect disappears is $\tau_i(T) \approx \tau_e$ so that the WL theory is in principle restricted to low temperatures and the maximum in the $\rho(T)$, and the nonmetallic NTC resistivity above the maximum both occur within the ballistic (Boltzmann) regime with $\tau_e < \tau_i$ (or even $\tau_e \ll \tau_i$). This is hard to justify for the δ-$FeZn_{10}$, where the resistivity maximum appears at a temperature as high as 220 K. In contrast, the SCC model is applicable at any temperature; the resistivity maximum appears at the transition from the ballistic (Boltzmann) to the diffusive (non-Boltzmann) type of electron motion and the high-temperature NTC resistivity occurs in the regime $\tau_e \gg \tau_i$ that can hold to arbitrary high temperatures. This favors the use of the SCC model over the WL model.

B. Magnetoresistance

The magnetic field-dependence of the magnetoresistance $\Delta\rho(B)/\rho$ has been theoretically elaborated in detail for the WL model,[24,30] and the theory was successfully applied to several icosahedral and decagonal Al-based quasicrystals.[31–33] For the SCC model, no theory of the magnetoresistance exists at present. The WL theory predicts that $\Delta\rho(B)/\rho$ starts as B^2 in the "low" field, whereas at "high" field it may give a $\sqrt{B}$ or weaker dependence. Here the words "low" and "high" field are used for when we observe a B^2 dependence or not, with no clear indication on the magnitude of the field where the change happens. The magnetic-field effects disappear with increasing temperature. Since the formerly discussed analysis of the temperature-dependent electrical resistivity of δ-$FeZn_{10}$ suggests inadequacy of the WL model in this case, we do not apply fitting of the field-dependent magnetoresistance data from Fig. 4(b) with the WL theory (that contains many fit parameters) but only give some qualitative discussion. At all investigated temperatures, the $\Delta\rho(B)/\rho$ data measured in the field range between 0- and 9-T field show approximately linear field dependence with no clear indication of a B^2 dependence at low field.

The temperature-dependent magnetoresistance $\Delta\rho/\rho$ in $B = 9$ T, shown in the inset of Fig. 4(b), has been analyzed phenomenologically by a model function

$$\frac{\Delta\rho}{\rho} = \left(\frac{a}{T - T'}\right)^{\beta}. \tag{7}$$

This form fits well the experimental data [solid curve in the inset of Fig. 4(b)] by using the fit parameter values $a = 121.5$ K, $T' = -104$ K, and $\beta = 3.0$. Here we emphasize that Eq. (7) should be considered merely as a convenient power-law functional form that reproduces well the experimental temperature-dependent magnetoresistance data of the δ-$FeZn_{10}$, without any deeper physical background.

C. Thermoelectric power and Hall coefficient

Unlike the electrical conductivity, which is proportional to the square of the electric charge ($\sigma \propto e^2$) and hence does not distinguish between the negative electron-type carriers ($-e$) and the positive hole-type carriers ($+e$), the thermopower S and the Hall coefficient R_H distinguish between the electrons and holes, as the charge in their expressions appears as e or $1/e$, respectively. S and R_H are thus much more sensitive to the details of the Fermi surface that determines the electronic transport coefficients.

The positive R_H of δ-$FeZn_{10}$ shown in Fig. 6 suggests that holes are the majority charge carriers, whereas the negative thermopower S of Fig. 5 offers the opposite conclusion that the charge is carried by the electrons. This apparent contradiction can be resolved by considering the details of the Fermi surface. Since the Fermi surface of the δ-$FeZn_{10}$ phase has not been determined as yet, we are unable to make quantitative analysis. However, opposite-sign $S < 0$ and $R_H > 0$ are not uncommon in the literature. This situation was discussed for the high-T_c cuprates,[34] where the electrons form an unusual state in which the Hall (cyclotron) mass parallel to the Fermi surface is holelike (<0), but the transport mass perpendicular to it is electronlike (>0). The electronlike transport mass contributes to negative S, while the holelike Hall mass results in positive R_H. A similar situation was found also for the Y-phase Al-Co-Ni decagonal approximant phase,[35] where the highly anisotropic Fermi surface was shown to be composed of eleven branches, and in the PdGa intermetallic phase.[36]

V. CONCLUSIONS

The δ-$FeZn_{10}$ phase in the zinc-rich domain of the Fe-Zn system possesses high structural complexity typical of CMAs: a large unit cell comprising 556 atoms, polyhedral atomic order with icosahedrally coordinated environments, fractionally occupied lattice sites, and statistically disordered atomic clusters that introduce intrinsic disorder into the structure. Structural disorder results in suppression of the electrical- and heat-transport phenomena, making δ-$FeZn_{10}$ poor electrical and thermal conductor. Structural complexity results in complex electronic structure that is reflected in the opposite signs of the thermoelectric power and the Hall coefficient. The δ-$FeZn_{10}$ phase is paramagnetic down to the temperature of 2 K with a significant interspin coupling of AFM type. The specific heat indicates the formation of short-range-ordered spin clusters at low temperatures, very likely a precursor of a phase transition to a collective magnetic state that would take place below our lowest investigated temperature of 2 K. The magnetoresistance

of δ-$FeZn_{10}$ is sizeable, amounting to 1.5% at 2 K in a 9-T field. The temperature-dependent electrical resistivity exhibits a maximum at about 220 K, and its temperature dependence can be explained by the theory of slow charge carriers, applicable to metallic systems with weak dispersion of the electronic bands, where the electron motion changes from ballistic to diffusive upon heating.

ACKNOWLEDGMENTS

This work was done within the activities of the European Integrated Center for the Development of New Metallic Alloys and Compounds (C-MAC). J.I., P.P., and A.S. acknowledge support by the Croatian Ministry of Science, Education and Sports, Grant No. 035-0352826-2848.

*Permanent address: Department of Physics, University of Osijek, Trg Ljudevita Gaja 6, HR-31000 Osijek, Croatia.

†Corresponding author: jani.dolinsek@ijs.si

[1] See, for a review, K. Urban and M. Feuerbacher, J. Non-Cryst. Solids **334 & 335**, 143 (2004).

[2] L. Pauling, J. Am. Chem. Soc. **45**, 2777 (1923).

[3] L. Pauling, Am. Sci. **43**, 285 (1955).

[4] G. Bergman, J. L. T. Waugh, and L. Pauling, Acta Crystallogr. **10**, 254 (1957).

[5] M. Boudard, H. Klein, M. de Boissieu, M. Audier, and H. Vincent, Philos. Mag. A **74**, 939 (1996).

[6] H. Klein, M. Audier, M. Boudard, M. de Boissieu, L. Behara, and M. Duneau, Philos. Mag. A **73**, 309 (1996).

[7] M. Feuerbacher, C. Thomas, and K. Urban, in *Quasicrystals, Structure and Physical Properties*, edited by H.-R. Trebin (Wiley-VCH, Weinheim, 2003), p. 2.

[8] S. Samson, Acta Crystallogr. **19**, 401 (1965).

[9] S. Samson, in *Developments in the Structural Chemistry of Alloy Phases*, edited by B. C. Giessen (Plenum, New York, 1969), p. 65.

[10] M. Feuerbacher, C. Thomas, J. P. A. Makongo, S. Hoffmann, W. Carrillo-Cabrera, R. Cardoso, Yu. Grin, G. Kreiner, J.-M. Joubert, Th. Schenk *et al.*, Z. Kristallogr. **222**, 259 (2007).

[11] G. Kreiner and H. F. Franzen, J. Alloys Compd. **261**, 83 (1997).

[12] F. J. Edler, V. Gramlich, and W. Steurer, J. Alloys Compd. **269**, 7 (1998).

[13] R. Cerny, M. Francois, K. Yvon, D. Jaccard, E. Walker, V. Petricek, I. Cisarova, H.-U. Nissen, and R. Wessiken, J. Phys.: Condens. Matter **8**, 4485 (1996).

[14] M. Conrad, B. Harbrecht, T. Weber, D. Y. Jung, and W. Steurer, Acta Crystallogr. Sec. B **65**, 318 (2009).

[15] See, e.g., C. Janot, *Quasicrystals*, 2nd ed. (Clarendon, Oxford, 1994), p. 1.

[16] C. H. E. Belin and R. C. H. Belin, J. Solid State Chem. **151**, 85 (2000).

[17] J. K. Brandon, R. Y. Brizard, P. C. Chieh, R. K. McMillan, and W. B. Pearson, Acta Crystallogr. Sec. B **30**, 1412 (1974).

[18] O. Kubaschewski, *Phase Diagram of Binary Iron Alloys* (ASM International, Materials Park, OH, 1993), p. 459.

[19] G. F. Bastin, F. J. J. van Loo, and G. D. Rieck, Z. Metallk. **65**, 656 (1974).

[20] G. F. Bastin, F. J. J. van Loo, and G. D. Rieck, Z. Metallk. **68**, 359 (1977).

[21] See, e.g. U. Mizutani, *Introduction to the Electron Theory of Metals* (Cambridge University Press, Cambridge, 2001), p. 43.

[22] U. Mizutani, *Introduction to the Electron Theory of Metals* (Cambridge University Press, Cambridge, 2001), p. 299.

[23] G. Trambly de Laissardière, J.-P. Julien, and D. Mayou, Phys. Rev. Lett. **97**, 026601 (2006).

[24] H. Fukuyama and K. Hoshino, J. Phys. Soc. Jpn. **50**, 2131 (1981).

[25] J. Dolinšek, P. Jeglič, M. Komelj, S. Vrtnik, A. Smontara, I. Smiljanić, A. Bilušić, J. Ivkov, D. Stanić, E. S. Zijlstra, B. Bauer, and P. Gille, Phys. Rev. B **76**, 174207 (2007).

[26] J. Dolinšek, S. Vrtnik, A. Smontara, M. Jagodič, Z. Jagličić, B. Bauer, and P. Gille, Philos. Mag. **88**, 2145 (2008).

[27] J. Dolinšek, M. Wencka, M. Jagodič, Z. Jagličić, S. Gottlieb-Schönmeyer, F. Ritter, and W. Assmus, Solid State Commun. **150**, 1629 (2010).

[28] M. Wencka, S. Jazbec, Z. Jagličić, S. Vrtnik, M. Feuerbacher, M. Heggen, S. Roitsch, and J. Dolinšek, Philos. Mag. **91**, 2756 (2011).

[29] M. Bobnar, P. Jeglič, M. Klanjšek, Z. Jagličić, M. Wencka, P. Popčević, J. Ivkov, D. Stanić, A. Smontara, P. Gille, and J. Dolinšek, Phys. Rev. B **85**, 024205 (2012).

[30] P. A. Lee and T. V. Ramakrishnan, Phys. Rev. B **26**, 4009 (1982).

[31] See, for a review, Ö. Rapp, Electronic transport properties of quasicrystals—experimental results, in *Physical Properties of Quasicrystals*, edited by Z. M. Stadnik (Springer-Verlag, Berlin, 1999), pp. 127–167.

[32] P. Lindqvist, P. Lanco, C. Berger, A. G. M. Jansen, and F. Cyrot-Lackmann, Phys. Rev. B **51**, 4796 (1995).

[33] A. Sahnoune, J. O. Ström-Olsen, and A. Zaluska, Phys. Rev. B **46**, 10629 (1992).

[34] Y. Kubo, Phys. Rev. B **50**, 3181 (1994).

[35] A. Smontara, I. Smiljanić, J. Ivkov, D. Stanić, O. S. Barišić, Z. Jagličić, P. Gille, M. Komelj, P. Jeglič, M. Bobnar, and J. Dolinšek, Phys. Rev. B **78**, 104204 (2008).

[36] M. Klanjšek, A. Gradišek, A. Kocjan, M. Bobnar, P. Jeglič, M. Wencka, Z. Jagličić, P. Popčević, J. Ivkov, A. Smontara, P. Gille, M. Armbrüster, Yu. Grin, and J. Dolinšek, J. Phys.: Condens. Matter **24**, 085703 (2012).